Eur. Phys. J. A **25**, 23–27 (2005)
DOI 10.1140/epja/i2005-10066-6

THE EUROPEAN PHYSICAL JOURNAL A

Shape evolution for Sm isotopes in relativistic mean-field theory

J. Meng[1,2,3,a], W. Zhang[1], S.G. Zhou[2,1,3], H. Toki[4], and L.S. Geng[1,4]

[1] School of Physics, Peking University, Beijing 100871, PRC
[2] Institute of Theoretical Physics, Chinese Academy of Sciences, Beijing 100080, PRC
[3] Center of Theoretical Nuclear Physics, National Laboratory of Heavy Ion Accelerator, Lanzhou 730000, PRC
[4] Research Center for Nuclear Physics (RCNP), Osaka University, Ibaraki, Osaka 567-0047, Japan

Received: 11 January 2005 / Revised version: 5 May 2005 /
Published online: 20 June 2005 –
Communicated by G. Orlandini

Abstract. The evolution of shape from the spherical to the axially deformed shapes in the Sm isotopes is investigated microscopically in relativistic mean-field theory. The microscopic and self-consistent quadrupole deformation constrained relativistic mean-field calculations show a clear shape change for the even-even Sm isotopes with $N = 82$–96. The potential surfaces for ^{148}Sm, ^{150}Sm and ^{152}Sm are found to be relatively flat, which may be the possible critical-point nuclei. By examining the single-particle spectra and nearest-neighbor spacing distribution of the single-particle levels, one finds that the single-particle levels in ^{148}Sm ,^{150}Sm, and ^{152}Sm distribute more uniformly.

PACS. 21.10.-k Properties of nuclei; nuclear energy levels – 21.60.Jz Hartree-Fock and random-phase approximations – 21.60.Fw Models based on group theory – 21.10.Re Collective levels

The equilibrium shapes for finite many-body systems such as atomic nucleus, atom, molecule, etc. have been a hot topic in the past several decades. These shapes are normally not rigid and change as a function of the number of their constituents. Sometimes these changes can be quite abrupt and exhibit phase transitional and critical-point behavior similar to that found in a wide variety of many-body systems, though the concept of phase transition is only approximate for finite systems.

Properties of a system in the transition region and in particular at the critical point can be found by solving the eigenvalue problem numerically. However, the transition region is difficult to interpret as they exhibit a complicated interplay of competing degrees of freedom. Yet such systems are in many respects the most important, as their structure defines the nature of the transition region itself.

Recently, the concept of such critical-point solutions has been introduced in the framework of the algebraic models, in which different shapes (phases) correspond to dynamic symmetries of some algebraic structure G and the phase transition corresponds to the breaking of the dynamical symmetries. In the Interacting Boson Model [1] $G \equiv U(6)$ and there are three dynamical symmetries characterized by the first algebra in the chain originating from $U(6)$, that is $U(5)$, $SU(3)$, and $SO(6)$, with spherical, axially deformed, and γ-unstable shapes. Experimental examples of all three types of symmetries can be found in nuclei, *e.g.*, the $U(5)$ nuclei can occur near closed shells, $SU(3)$ nuclei can occur in the middle of two neighboring shells, and the $O(6)$ limit tends to occur in nuclei with particle-hole configuration. The phase transition between spherical $U(5)$ and axially deformed shapes $SU(3)$ is of the first order [2,3]. The phase/shape transition region is characterized by a pronounced β softness [4]. This characteristic leads to the analytic solution for critical-point nuclei, called $X(5)$ for the axially symmetric case, and is based on analytic solutions of the Schrödinger equation corresponding to a geometric (Bohr) Hamiltonian with a square-well potential [5]. First examples of $X(5)$ symmetry in transitional nuclei have been found in ^{152}Sm [6], ^{150}Nd [7], and others in different nuclear regions [8–15]. From the theoretical point of view, the nuclei which correspond the critical point of the phase transition have been discussed with different potential shape in refs. [16–19].

The critical-point symmetries provide a classification of states and analytic expressions for observables in regions where the structure changes most rapidly [20]. The idea of $X(5)$ critical-point symmetry can be visualized in terms of two coexisting minima in the potential surface, a spherical minimum and a deformed one, whose energy difference varies with nucleon number. Although phase transition and critical point have been discussed in finite systems for many years, their microscopical investigations are still missing. In fact, a microscopic study is

[a] e-mail: mengj@pku.edu.cn

necessary and essential for us to understand and recognize where and how these symmetries occur. The present paper aims at this problem and microscopically studies the $X(5)$ critical-point symmetry in actually physical systems, namely atomic nuclei.

The relativistic mean-field (RMF) theory [21] has received wide attention because of its successful description of many nuclear phenomena during the past years [22]. In particular, the exotic halo phenomena can be understood self-consistently after a proper treatment of the continuum effect [23–25], the long-existing problem for the origin of pseudo-spin symmetry in nuclei has been given naturally [26–28], and a new symmetry —the spin symmetry for the spectrum of an antinucleon has been predicted [29, 30]. It is very interesting to investigate the critical-point concept in atomic nuclei with this microscopic and self-consistent RMF theory which will show that ^{148,150,152}Sm are excellent empirical manifestations of this critical-point structure.

The basic Ansatz of the RMF theory is a Lagrangian density where nucleons are described as Dirac particles which interact via the exchange of various mesons including the isoscalar-scalar σ-meson, the isoscalar-vector ω-meson and the isovector-vector ρ-meson. The effective Lagrangian density considered is written in the form

$$\begin{aligned}\mathcal{L} = & \bar{\psi}_i \left(i\partial\!\!\!/ - M\right)\psi_i + \frac{1}{2}\partial_\mu\sigma\partial^\mu\sigma - U(\sigma) - g_\sigma\bar{\psi}_i\sigma\psi_i \\ & - \frac{1}{4}\Omega_{\mu\nu}\Omega^{\mu\nu} + \frac{1}{2}m_\omega^2\omega_\mu\omega^\mu - g_\omega\bar{\psi}_i\omega\!\!\!/\psi_i \\ & - \frac{1}{4}\vec{R}_{\mu\nu}\vec{R}^{\mu\nu} + \frac{1}{2}m_\rho^2\vec{\rho}_\mu\vec{\rho}^\mu - g_\rho\bar{\psi}_i\vec{\rho}\!\!\!/\vec{\tau}\psi_i \\ & - \frac{1}{4}F_{\mu\nu}F^{\mu\nu} - e\bar{\psi}_i\frac{1-\tau_3}{2}A\!\!\!/\psi_i, \end{aligned} \quad (1)$$

where $\bar{\psi} = \psi^\dagger\gamma^0$ and ψ is the Dirac spinor. Other symbols have their usual meanings.

The Dirac equation for the nucleons and the Klein-Gordon–type equations for the mesons and the photon are given by the variational principle and can be solved by expanding the wave functions in terms of the eigenfunctions of a deformed axially symmetric harmonic-oscillator potential [31] or a Woods-Saxon potential [32].

The potential energy curve can be calculated microscopically by the constrained RMF theory. The binding energy at a certain deformation is obtained by constraining the quadrupole moment $\langle Q_2\rangle$ to a given value μ_2 in the expectation value of the Hamiltonian [33],

$$\langle H'\rangle \;=\; \langle H\rangle + \frac{1}{2}C_\mu\left(\langle Q_2\rangle - \mu_2\right)^2, \quad (2)$$

where C_μ is the constraint multiplier. The deformation parameter β_2 is obtained from the calculated quadrupole moments $\langle Q_2\rangle$ for the protons and neutrons through

$$\langle Q_2\rangle = \langle Q_{2p}\rangle + \langle Q_{2n}\rangle = \frac{3}{\sqrt{5\pi}}AR_0^2\beta_2, \quad (3)$$

with $R_0 = 1.2A^{1/3}$.

Table 1. The total binding energy and the quadrupole deformation β_2 of the ground states of $^{144-158}$Sm calculated by the constrained RMF theory with effective interactions NL1, NL3, NLSH and TM1. Available data are included for comparison.

E (MeV)	EXP [34]	NL1	NL3	NLSH	TM1
^{144}Sm	1195.74	1201.28	1198.34	1200.20	1202.03
^{146}Sm	1210.91	1213.83	1211.79	1214.00	1215.51
^{148}Sm	1225.40	1225.95	1225.48	1227.95	1230.04
^{150}Sm	1239.25	1239.59	1239.29	1241.09	1243.47
^{152}Sm	1253.11	1252.78	1253.54	1255.39	1256.18
^{154}Sm	1266.94	1265.50	1267.54	1269.59	1268.67
^{156}Sm	1279.99	1276.98	1280.05	1282.26	1281.58
^{158}Sm	1291.98	1287.57	1291.73	1293.99	1293.08
β_2	EXP [35]	NL1	NL3	NLSH	TM1
^{144}Sm	0.09	0.00	0.00	−0.01	−0.00
^{146}Sm		0.05	0.06	0.08	−0.03
^{148}Sm	0.14	0.15	0.14	0.14	0.10
^{150}Sm	0.19	0.25	0.23	0.21	0.13
^{152}Sm	0.31	0.34	0.30	0.28	0.18
^{154}Sm	0.34	0.35	0.33	0.32	0.33
^{156}Sm		0.36	0.34	0.33	0.32
^{158}Sm		0.36	0.35	0.34	0.33

For the nuclei studied in this paper, the full $N = 20$ deformed harmonic-oscillator shells are taken into account. This basis is large enough to produce a good convergence on the binding energy and the deformation in the numerical calculation. The converged deformation is not sensitive to the deformation parameter β_0 of the harmonic-oscillator basis in a reasonable range due to the large basis. By varying μ_2, the binding energy at different deformation is obtained. The pairing correlation is treated by the constant gap BCS approximation where the pairing gap is taken as $12/\sqrt{A}$.

The binding energy and the quadrupole deformation for the ground state are listed in table 1. The constrained RMF calculations are carried out with effective interactions NL1 [36], NLSH [37], TM1 [38], and NL3 [39]. For the binding energy, the data is well reproduced within 0.5%. Particularly, excellent agreement (within 1 MeV) is obtained for the binding energy in $^{146-158}$Sm with NL3. Even for neutron magic nuclei ^{144}Sm, the difference between the RMF calculation and the data is less than 3 MeV, *i.e.*, less than 0.3% relatively. The spherical shapes in ^{144,146}Sm and the weakly deformed ^{148}Sm are well reproduced. The deformations in $^{150-158}$Sm are a little overestimated by the theoretical calculations.

Figures 1, 2, 3, and 4 show the potential energy curves for $^{144-158}$Sm from constrained RMF calculations with effective interactions NL1, NL3, NLSH, and TM1. In each figure the energy for the ground state is taken as a reference. Similar patterns are found for all the effective interactions. The ground state of ^{144}Sm is found to be spherical and has about a 12 MeV stiff barrier against deformation. Although the ground state of ^{146}Sm is still spherical, its barrier becomes lower and is around 8 MeV against the deformation. With the increase of the neutron number,

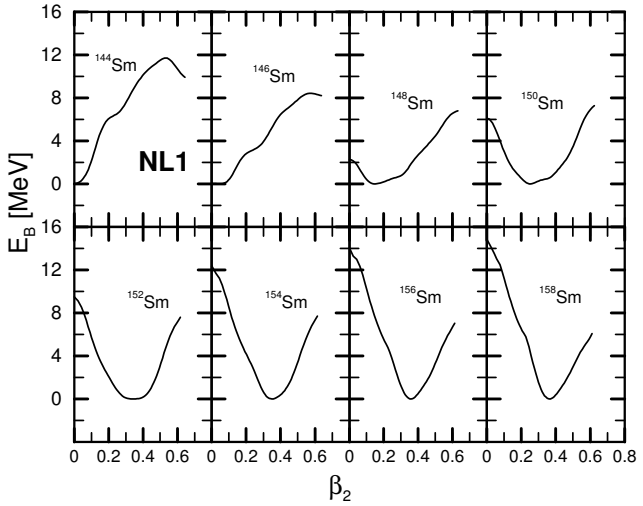

Fig. 1. The potential energy curves for $^{144-158}$Sm obtained by the constrained RMF theory with effective interaction NL1. The ground-state binding energy is taken as a reference.

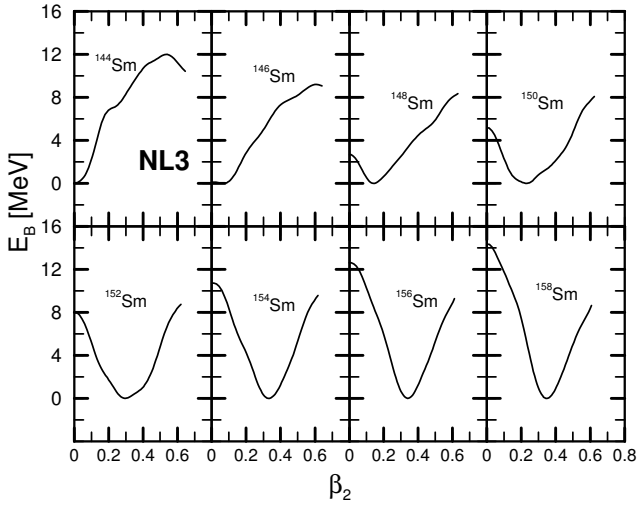

Fig. 2. The same as fig. 1, but with NL3.

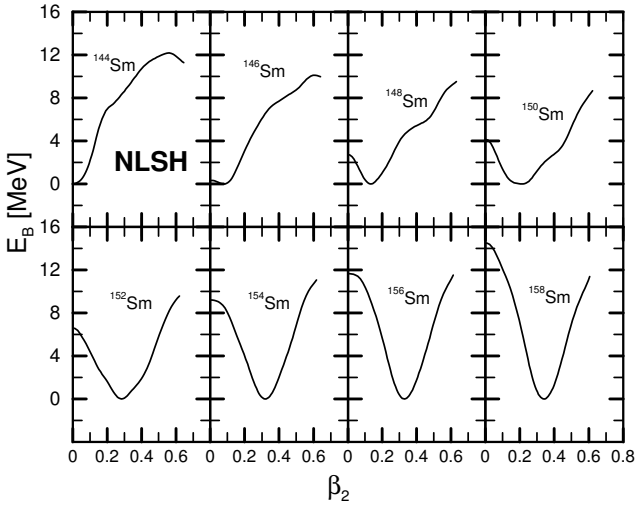

Fig. 3. The same as fig. 1, but with NLSH.

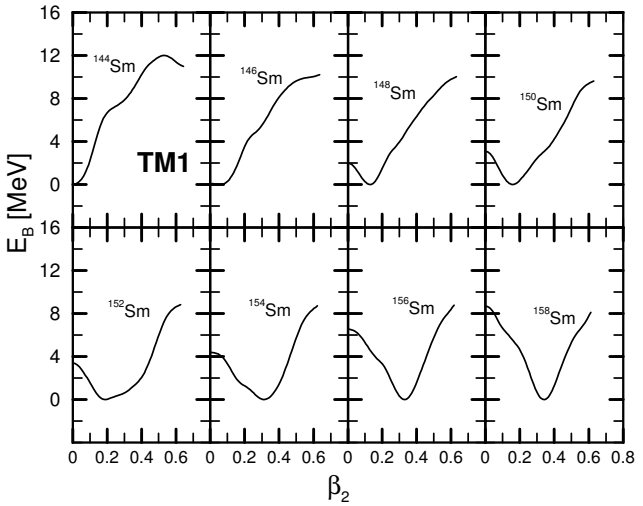

Fig. 4. The same as fig. 1, but with TM1.

the ground state gradually moves toward the deformed side and the potential energy curve becomes softer. Finally well-deformed $^{154-158}$Sm are reproduced.

To examine how the shape of the Sm isotopes changes with the neutron number, the differences of the binding energy between the ground state and the state with the spherical shape for Sm isotopes are presented in table 2 in the constrained RMF theory with effective interactions NL1, NL3, NLSH, and TM1. These differences can tell us how soft the nucleus is against deformation and may give us a hint on the phase transition of the nuclear shape. From $^{144-158}$Sm, the energy differences between the ground state and the state with spherical-shape change from 0 to 15 MeV. There are two jumps in the energy differences. The first jump appears at ^{148}Sm and the second at ^{154}Sm, which suggests the shape change from spherical to critical-point nuclei, and finally to axially deformed nuclei. The potential energy curves for ^{148}Sm, ^{150}Sm, and ^{152}Sm are relatively flat, *i.e.*, they are β_2-soft nuclei in the transition region between spherical and axially symmetric deformed nuclei.

Table 2. The difference of the binding energy between the spherical state and the ground state in units of MeV calculated by the constrained RMF theory with effective interactions NL1, NL3, NLSH and TM1 for $^{144-158}$Sm.

	NL1	NL3	NLSH	TM1
^{144}Sm	0.00	0.00	0.00	0.00
^{146}Sm	0.02	0.11	0.33	0.07
^{148}Sm	2.26	2.67	2.72	1.98
^{150}Sm	6.11	5.19	4.13	3.08
^{152}Sm	9.51	8.02	6.59	3.38
^{154}Sm	12.33	10.73	9.20	4.37
^{156}Sm	14.10	12.61	11.64	6.53
^{158}Sm	14.80	14.36	14.51	8.68

One of the merits of microscopic models such as RMF theory is that it can provide detailed information on single-particle levels, shell structure etc., which are very

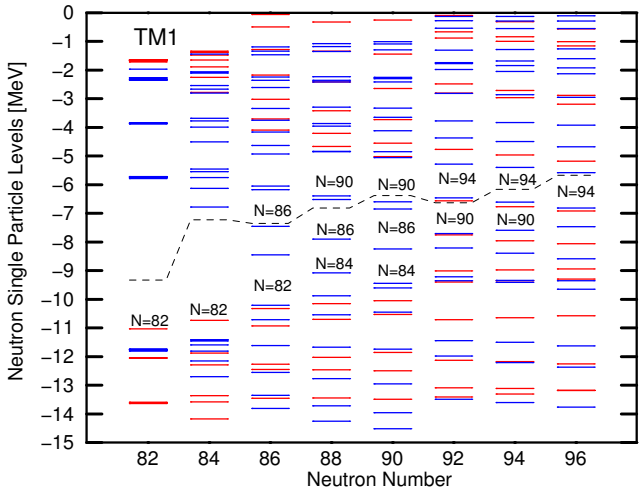

Fig. 5. The single-neutron levels for $^{144-158}$Sm obtained by the constrained RMF theory with effective interaction TM1.

important for us to discuss nuclear structure, examine the deformation-driving effect and understand the physical origin for the critical-point nuclei. In fig. 5 the single-neutron levels for $^{144-158}$Sm lying between -15 and 0 MeV are shown. The Fermi levels are presented by the dashed line. This figure presents results calculated with effective interaction TM1. The other three effective interactions give similar single-particle structure thus not presented here.

From fig. 5 one finds a consistency between the shell structure evolution and the shape evolution in Sm isotopes with increasing neutron number. Namely, for ^{144}Sm, spherical symmetry is better restored. The deformation develops with N increasing. The deformation in ^{146}Sm is still small and the energy gap with $N = 82$ can be clearly seen from the single-particle spectra. The critical-point nuclei $^{148-152}$Sm belong to a transition area in which the $N = 82$ gaps still exist but are much smaller than that in ^{144,146}Sm. Starting from ^{154}Sm, the gap with $N = 82$ disappears. Meanwhile a deformed gap develops around $N = 94$. Correspondingly, we observe the well-deformed $^{154-158}$Sm. The single-particle spectra in critical-point nuclei $^{148-152}$Sm are more uniformly distributed, which are quite different from those in either $U(5)$ spherical or $SU(3)$ well-deformed nuclei where there are obvious energy gaps. This characteristic in microscopic shell structure can be viewed as the signature of the critical-point symmetry.

The nearest-neighbor spacing distribution of the single-neutron levels in the interval $[0, -30]$ MeV is shown in fig. 6 which presents more clearly the shell structure evolution with increasing neutron number. As seen in fig. 6, most nearest-neighbor spacings are within $[0, 0.4]$ MeV. However, for ^{144}Sm and ^{146}Sm, there are several levels lying 4–5 MeV away from their neighbors. These large spacings correspond, of course, to large energy gaps between neighboring shells. With increasing N, the levels distribute more evenly, as shown in the figure, and one finds roughly Poisson-like distributions in ^{148,150,152}Sm. For well-deformed nuclei, *e.g.* ^{158}Sm,

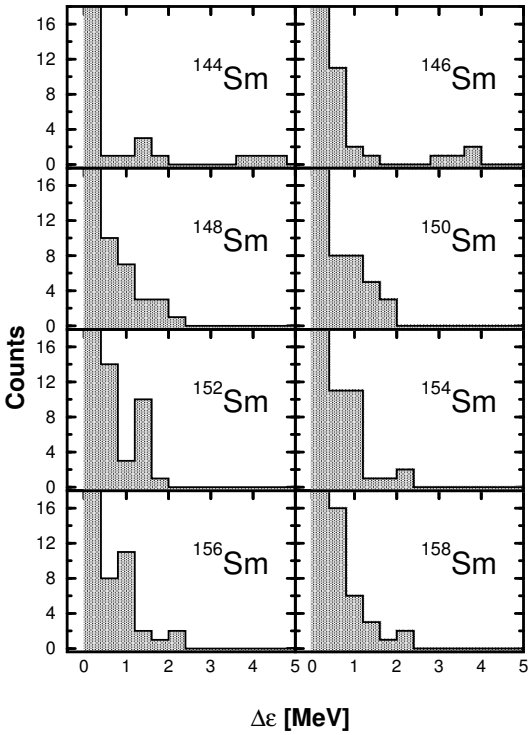

Fig. 6. The nearest-neighbor spacing distribution of the single-particle levels in the interval [0, −30] MeV for neutron in $^{144-158}$Sm calculated by the RMF theory with effective interaction TM1. The energy step is taken as 0.4 MeV.

large energy gaps develop again and the nearest-neighbor spacing distributions deviate Poisson-like ones. Thus, the nearest-neighbor spacing distribution of the single-particle levels seems to provide one of the criteria for identifying critical-point nuclei.

In summary, the evolution of shape from the spherical to the axially deformed shapes in the Sm isotopes is investigated microscopically in relativistic mean-field theory. The even-even Sm isotopes, $^{144-158}$Sm, are studied by the constrained relativistic mean-field theory with all the most successful effective interactions, *i.e.*, NL1, NL3, NLSH and TM1. The RMF calculation reproduces very well the data of the binding energy and the deformation for the ground states. ^{148}Sm ,^{150}Sm, and ^{152}Sm are found to be soft against β deformation in their corresponding potential energy curves. By examining the single-particle spectra and nearest-neighbor spacing distribution of the single-particle levels, one finds that the single-particle levels in ^{148}Sm ,^{150}Sm, and ^{152}Sm distribute more uniformly.

We thank Victor Zamfir for helpful discussions and useful comments. This work was partly supported by the Major State Basic Research Development Program under contract No. G2000077407 and the National Natural Science Foundation of China under grant Nos. 10435010, 10221003, and 10475003, the Doctoral Program Foundation from the Ministry of Education in China, and the Knowledge Innovation Project of Chinese Academy of Sciences under contract No. KJCX2-SW-N02.

References

1. F. Iachello, A. Arima, *The Interacting Boson Model* (Cambridge University Press, Cambridge, England, 1987).
2. A.E.L. Dieperink, O. Scholten, F. Iachello, Phys. Rev. Lett. **44**, 1747 (1980).
3. D.H. Feng, R. Gilmore, S.R. Deans, Phys. Rev. C **23**, 1254 (1981).
4. F. Iachello, N.V. Zamfir, F. Iachello, Phys. Rev. Lett. **81**, 1191 (1998).
5. F. Iachello, Phys. Rev. Lett. **87**, 052502 (2001).
6. R.F. Casten, N.V. Zamfir, Phys. Rev. Lett. **87**, 052503 (2001).
7. R. Krücken *et al.*, Phys. Rev. Lett. **88**, 232501 (2002).
8. M.A. Caprio *et al.*, Phys. Rev. C **66**, 054310 (2002).
9. P.G. Bizzeti, A.M. Bizzeti-Sona, Phys. Rev. C **66**, 031301(R) (2002).
10. C. Hutter *et al.*, Phys. Rev. C **67**, 054315 (2003).
11. R.M. Clark *et al.*, Phys. Rev. C **68**, 037301 (2003).
12. R. Bijker, R.F. Casten, N.V. Zamfir, E.A. McCutchan, Phys. Rev. C **68**, 064304 (2003).
13. C. Fransen, N. Pietralla, A. Linnemann, V. Werner, R. Bijker, Phys. Rev. C **69**, 014313 (2004).
14. D. Tonev, A. Dewald, T. Klug, P. Petkov, J. Jolie, A. Fitzler, O. Moller, S. Heinze, P. von Brentano, R.F. Casten, Phys. Rev. C **69**, 034334 (2004).
15. R. Bijker, R.F. Casten, N.V. Zamfir, E.A. McCutchan, Phys. Rev. C **69**, 059901(E) (2004).
16. M.A. Caprio, Phys. Rev. C **69**, 044307 (2004).
17. D. Bonatsos, D. Lenis, N. Minkov, D. Petrellis, P.P. Raychev, P.A. Terziev, Phys. Rev. C **70**, 024305 (2004).
18. N. Pietralla, O.M. Gorbachenko, Phys. Rev. C **70**, 011304(R) (2004).
19. P.G. Bizzeti, A.M. Bizzeti-Sona, Eur. Phys. J. A **20**, 179 (2004); Phys. Rev. C **70**, 064319 (2004).
20. A. Leviatan, J.N. Ginocchio, Phys. Rev. Lett. **90**, 212501 (2003).
21. B. Serot, J.D. Walecka, Adv. Nucl. Phys. **16**, 1 (1986).
22. P. Ring, Prog. Part. Nucl. Phys. **37**, 193 (1996).
23. J. Meng, P. Ring, Phys. Rev. Lett. **77**, 3963 (1996).
24. J. Meng, Nucl. Phys. A **635**, 3 (1998).
25. J. Meng, P. Ring, Phys. Rev. Lett. **80**, 460 (1998).
26. J.N. Ginocchio, Phys. Rev. Lett. **78**, 436 (1997).
27. J. Meng, K. Sugawara-Tanabe, S. Yamaji, P. Ring, A. Arima, Phys. Rev. C **58**, R628 (1998).
28. J. Meng, K. Sugawara-Tanabe, S. Yamaji, A. Arima, Phys. Rev. C **59**, 154 (1999).
29. J.N. Ginocchio, Phys. Rep. **315**, 231 (1999).
30. S.G. Zhou, J. Meng, P. Ring, Phys. Rev. Lett. **91**, 262501 (2003).
31. Y. Gambhir, P. Ring, A. Thimet, Ann. Phys. (N.Y.) **198**, 132 (1990).
32. S.G. Zhou, J. Meng, P. Ring, Phys. Rev. C **68**, 034323 (2003).
33. P. Ring, P. Schuck, *The Nuclear Many-Body Problem* (Springer, 1980).
34. G. Audi, O. Bersillon, J. Blachot, Nucl. Phys. A **624**, 1 (1997).
35. S. Raman, C.W. Nestor jr., P. Tikkanen, At. Data Nucl. Data Tables **78**, 1 (2001).
36. P.G. Reinhard, M. Rufa, J. Maruhn, W. Greiner, J. Friedrich, Z. Phys. A **323**, 13 (1986).
37. M.M. Sharma, M.A. Nagarajan, P. Ring, Phys. Lett. B **312**, 377 (1993).
38. Y. Sugahara, H. Toki, Nucl. Phys. A **579**, 557 (1994).
39. G.A. Lalazissis, J. König, P. Ring, Phys. Rev. C **55**, 540 (1997).